Evidence for strong f-d hybridization in intermetallic ferromagnet $CePdIn_2$

E. Carleschi,[1,*] B.P. Doyle,[1] J.L. Snyman,[2] E. Magnano,[3,1] S. Nappini,[3] I. Pis,[3,4] F. Bondino,[3] P. Peratheepan,[2,5] and A.M. Strydom[2]

[1] *Department of Physics, University of Johannesburg, PO Box 524, Auckland Park 2006, South Africa*
[2] *Highly Correlated Matter Research Group, Department of Physics, University of Johannesburg, PO Box 524, Auckland Park 2006, South Africa*
[3] *IOM-CNR Laboratorio TASC, S.S. 14 km 163.5, Area Science Park, 34149 Basovizza (TS), Italy*
[4] *Elettra-Sincrotrone Trieste S.C.p.A., S.S. 14 km 163.5, Area Science Park, 34149 Basovizza (TS), Italy*
[5] *Department of Physics, Eastern University, Vantharumoolai, Chenkalady 30350, Sri Lanka*

(Dated: December 16, 2015)

We have investigated the contribution of Ce $4f$ states to the electronic structure of the intermetallic ferromagnet $CePdIn_2$ by means of x-ray absorption spectroscopy and resonant and non-resonant photoemission spectroscopy. The line shape of the Ce $M_{5,4}$ absorption edge reveals the localized nature of the $4f$ states, and is consistent with a predominantly 3+ ionic state for Ce ions. Fitting of the Ce $3d$ core level gives a Ce $4f$ occupation number at room temperature of 0.92, which is in good agreement with the Ce effective magnetic moment of 2.20 μ_B (corresponding to $\sim 87\%$ of the free-electron moment) as calculated from the inverse magnetic susceptibility. Moreover, the hybridization strength between $4f$ and conduction electrons is found to be ~ 180 meV, revealing that $CePdIn_2$ is a strongly hybridized system. This is consistent with the results from the analysis of the resonant valence band photoemission measurements at both the $N_{5,4}$ and the M_5 edges, showing that the Ce $4f$ states are composed of the features predicted by the single impurity Anderson model, i.e. a broad $4f^0$ peak centred at 1.9 eV and two $4f^1$ spin-orbit states much closer to the Fermi level. The same spectra also show that the Ce $4f$ resonant spectral weight extends over a wide binding energy range, overlapping with that presumably occupied by the Pd $4d$ ligand states. This energy overlap is interpreted as a signature of the strong hybridization governing the system, which could possibly favour the emergence of long range ferromagnetism through the indirect exchange between localized $4f$ states mediated by highly dispersive d electrons.

PACS numbers: 71.20.Eh, 71.20.Lp, 78.70.Dm, 79.60.-i

INTRODUCTION

A large proportion of research into rare earth-based intermetallic compounds has been dominated by the study of many-body, cooperative phenomena such as new quantum states of matter, magnetic ordering, itinerant heavy fermion behaviour and unconventional superconductivity in Ce-based systems, which can be tuned by the change of the degree of hybridization between band electrons and the $4f$ electrons of Ce [1, 2]. An important protocol for understanding this variety of observed phenomena has been established by Doniach [3], where the relative strength of the Kondo and Ruderman-Kittel-Kasuya-Yosida (RKKY) interactions ultimately determine the ground state properties of the system.

Ternary indides of Ce and Pd in various stoichiometric configurations have provided fertile ground in which to study the consequences of the hybridization between rare earth f electrons and highly dispersive Pd d electron bands, characterized by a large radial extent of their wavefunction. There are almost twenty phases known to form in the Ce-Pd-In system [4]. Reported studies of the physical properties of CePdIn [5, 6], $CePdIn_2$ [7, 8], $CePd_2In$ [9, 10], $Ce_8Pd_{24}In$ [11], $Ce_4Pd_{10}In_{21}$ [12], $CePd_2In_4$ [13], $CePd_3In_2$ [14], Ce_2PdIn_8 [15–17] and $Ce_6Pd_{12}In_5$ [18] reveal a remarkable diversity of crystal structures and physical phenomena. For example, the co-occurrence of heavy fermion behaviour and magnetic order is found in CePdIn [5, 6], $Ce_8Pd_{24}In$ [11], $CePd_3In_2$ [14] and $Ce_6Pd_{12}In_5$ [18], while the nature of the heavy fermion superconducting state of Ce_2PdIn_8 is still actively pursued [15–17, 19, 20].

Amongst this variety, $CePdIn_2$ was the first Ce-containing compound discovered to form in the orthorhombic BRe_3-type structure [7]. $CePdIn_2$ has been reported to order ferromagnetically at $T_C = 10\,\mathrm{K}$, and to have a small Kondo temperature $T_K = 5\,\mathrm{K}$ [8]. The confluence of a ferromagnetic ground state and Kondo coupling happens quite rarely in the realm of Ce-based systems, and has contributed to instil interest in this particular compound. Above T_C electrical resistivity results for $CePdIn_2$ reveal predominantly metallic behaviour. The above suggests that the physical properties of this system could be understood in the framework of the RKKY interaction, where Ce $4f$ electrons are expected to have a localized nature, and that $CePdIn_2$ could consequently be described as a local moment metallic ferromagnet.

Despite this, important features regarding the physical properties of this compound still evade a complete de-

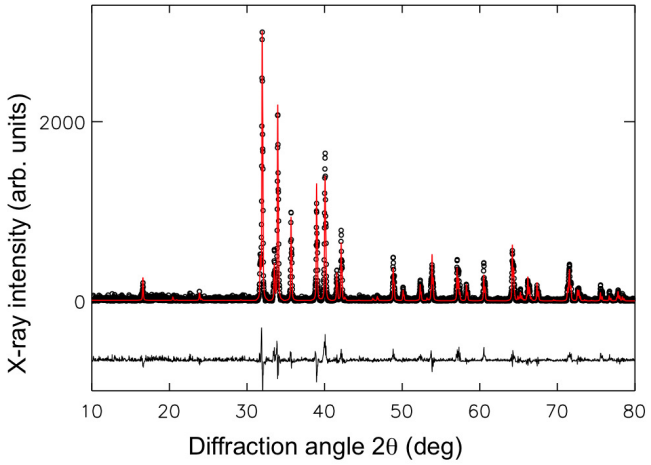

FIG. 1: (Color online) Powder x-ray diffractogram of annealed polycrystalline $CePdIn_2$ (black circles) and the simulated spectrum calculated from a full profile Rietveld refinement (red solid line). The residual spectrum is shown at the bottom of the graph (black solid line).

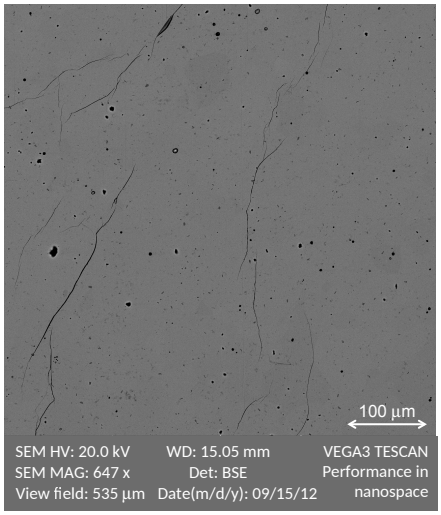

FIG. 2: SEM micrograph of a polished and carbon coated $CePdIn_2$ sample. This image has been measured at a magnification of 647x with a view field of 535 μm.

scription consistent with all the observables. In fact, the inverse magnetic susceptibility χ^{-1} (see Fig. 8) reveals that Curie-Weiss behaviour is present from 400 K down to the ferromagnetic phase transition temperature of 10 K. However, the associated effective magnetic moment is only $\sim 87\%$ of the theoretical value expected for trivalent Ce ions. The specific heat $C_P(T)$ (see Fig. 9) analyzed in terms of the three-level Schottky description offers some evidence in support of strong crystalline electric field (CEF) effects present in the system, while by contrast the magnetic susceptibility shows no evidence of CEF excitations. Furthermore, $C_P(T)$ shows that $CePdIn_2$ is a model mean field ferromagnet, implying that long-range magnetic correlations are already present at high temperature and are responsible for the establishment of an ordered magnetic state. Together with the inverse magnetic susceptibility this seems to imply a narrow critical region in the vicinity of the magnetic phase transition. The emerging of long-range magnetic order could suggest either a partial delocalization of the Ce $4f$ wave-function (which is not a novel feature in the framework of f-electron systems [21–25]) or hint to the pivotal role played by the interaction between Ce $4f$ and band electrons in this compound.

These results have inspired the electronic structure investigation reported in this study. We have probed the contribution of the Ce $4f$ states to the electronic structure in $CePdIn_2$ by means of x-ray absorption spectroscopy (XAS) across the Ce $M_{5,4}$ absorption edge, photoemission spectroscopy (PES) of the Ce $3d$ core level, and resonant photoemission spectroscopy (ResPES) at the Ce $N_{5,4}$ and M_5 edges. There are several examples in the literature where combining measurable bulk physical properties with electronic structure measurements in Ce-based intermetallic compounds has led to further unraveling of the full picture of the ground state properties of these systems (see for example Refs. [26–29]). The combined analysis of the Ce $M_{5,4}$ XAS and the Ce $3d$ core level has revealed the localized character of the Ce $4f$ wave-function that coexists with a strong f-d hybridization. The enhancement of the Ce $4f$ photoionisation cross section due to the resonance process has allowed us to unambiguously identify the contribution and the location of the Ce $4f$ states to the valence band, giving further insights into the degree of f-d hybridization in this compound.

EXPERIMENTAL DETAILS

Polycrystalline samples of $CePdIn_2$ were prepared from stoichiometric amounts of the constituent elements in an arc furnace under ultra-high purity argon atmosphere. The purity of Ce, Pd and In (in wt.%) was 99.99, 99.99 and 99.999 respectively. The cast samples were wrapped in Ta foil and annealed at 800°C for 14 days in an evacuated quartz ampoule. The crystalline structure and the chemical composition were checked by means of powder x-ray diffraction (XRD), scanning electron microscopy (SEM) and multi-spot energy dispersive spectroscopy (EDS). Fig. 1 shows the experimental powder x-ray diffractogram for $CePdIn_2$ together with the simulated spectrum calculated from a full profile Rietveld refinement using GSAS [30, 31]. The refined lattice parameters for the orthorhombic unit cell are (in Å) $a = 4.6191(1)$, $b = 10.6859(3)$ and $c = 7.4499(2)$, in good agreement with those reported by Ijiri, Di Salvo and Yamane [7]. Fig. 2 shows a SEM micrograph of a polished area of $CePdIn_2$, where the lack of

chemical contrast is taken to indicate a single bulk phase and a high degree of homogeneity. EDS elemental analysis revealed a stoichiometry (normalized to the atomic % of Ce) of $Ce_{1.0x(2)}Pd_{1.0y(2)}In_{2.0z(2)}$. No impurity phases were detected by either XRD or EDS. Taken together, these results indicate that $CePdIn_2$ formed in the desired phase and that impurity phases are absent to within the detection limits.

Photoemission and XAS measurements were acquired at the beamline BACH at Elettra [32], the Italian synchrotron radiation facility in Trieste. Samples were scraped with a diamond file in ultra high vacuum at a base pressure of 6×10^{-10} mbar, and kept at room temperature for the duration of the measurements. The pressure in the measurement chamber was stable at 5×10^{-10} mbar throughout the experiment. Photon energies were calibrated by measuring the Au $4f$ core level on a clean gold reference sample. The cleanliness of the sample surface was ensured by checking the C $1s$ and O $1s$ photoemission core levels throughout the measurements, as well as by checking the O $2p$ contribution to the valence band around 6 eV binding energy. Valence band measurements on an aged sample surface (i.e. 16 hours after scraping, shown in Fig. S1 of the Supplementary Information) have shown that the effect of surface contamination is to drastically suppress the spectral weight at the Fermi level (E_F), as well as to develop a broad peak located from 3.5 to 5 eV binding energy. In order to avoid this contribution to the valence band spectra, samples were scraped every 12 hours, and all measurements shown here (except for the XAS spectra in Fig. 3 (c) and (d)) were acquired within 10 hours from the latest scraping.

XAS spectra were measured in total electron yield (TEY) by measuring the drain current from the sample with a photon energy resolution of 200 meV. PES spectra were measured with a Scienta R3000 electron energy analyser. The angle between the incoming photon beam and the electron analyser's electrostatic lens axis was fixed at 60°, and the PES spectra were acquired in normal emission. The overall (photon+analyser) energy resolution was set to 300 meV for the Ce $3d$ core level, 80 meV for Ce $N_{5,4}$ ResPES and 250 meV for Ce $M_{5,4}$ ResPES.

With regards to the measurements reported in the Appendixes, the magnetic susceptibility was obtained using a SQUID-type magnetometer (MPMS, Quantum Design, San Diego) in an applied magnetic field H = 500 Oe, while the specific heat was obtained using the relevant measurement option of a Physical Properties Measurement System (PPMS, also from Quantum Design).

RESULTS AND DISCUSSION

Fig. 3(a) shows the Ce $M_{5,4}$ ($3d_{5/2,3/2} \rightarrow 4f$) XAS spectrum for $CePdIn_2$. The M_5 edge is formed from two low-intensity pre-peaks followed by two high-intensity

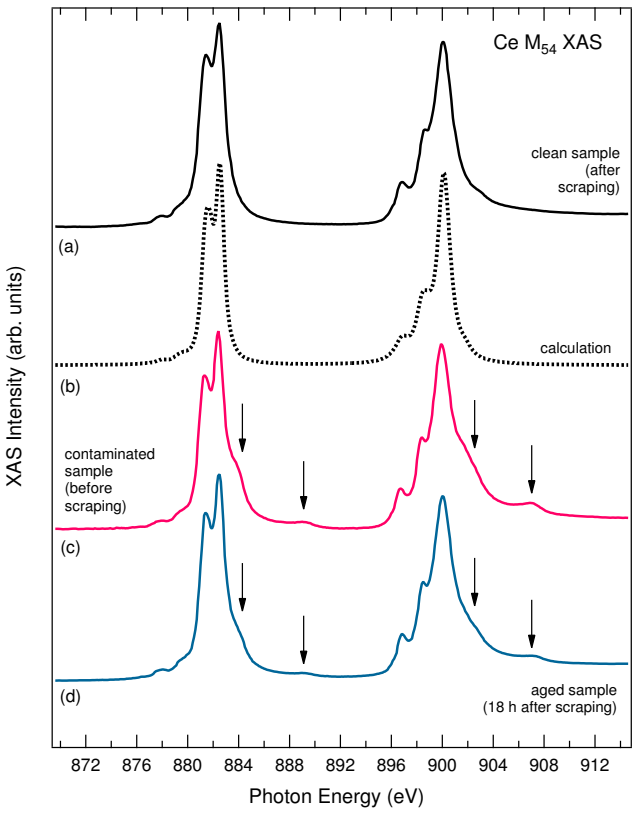

FIG. 3: (Color online) Ce $M_{5,4}$ XAS spectra for (a) a clean $CePdIn_2$ sample just after scraping, (c) a contaminated $CePdIn_2$ sample (i.e. measured before scraping in UHV) and (d) an aged $CePdIn_2$ sample measured 18 hours after scraping. The features that are signature of surface contamination are indicated with arrows in spectra (c) and (d). Spectrum (b) is the simulation of the $M_{5,4}$ edge for the Ce^{3+} ionic state, as explained in the main text; this is to be compared to spectrum (a) in this figure.

components located at 881.4 eV and 882.5 eV. The M_4 edge has a more intense feature at 900 eV, with two well defined shoulders on its low energy side (at 896.8 eV and 898.6 eV respectively) and a broad weak shoulder on its high energy side located at about 902.8 eV. The line shape of the $M_{5,4}$ edge resembles very well - in terms of both energy separation and intensity distribution of the various components - the calculation performed using Ligand Field Multiplet (LFM) formalism for the Ce^{3+} valence state shown in Fig. 3(b) (which is also in very good agreement with the results presented by Thole *et al.* in Ref. [33]). Our LFM simulation was carried out using the CTM4XAS 5.5 package based on the original code written by Cowan [34] and further developed by de Groot [35]. For the calculation of the Ce^{3+} spectrum, a transition from the $3d^{10}4f^1$ initial state to the $3d^9 4f^2$ final state configuration was considered, while the crystal field was not included because it is generally negligible

in f-systems [34]. The Slater integral F(ff) was reduced to 72%, while F(df) and G(df) were kept at 100%, and the 3d spin-orbit coupling parameter was set at 99% of the atomic Hartree-Fock values. A Gaussian broadening of 0.2 eV and Lorentzian broadenings of 0.3 and 0.5 eV were applied to M_5 and M_4 edges respectively, to take into account the instrumental broadening effect. The parameters used for the calculation of the theoretical XAS spectrum of Ce(III) $M_{5,4}$ edge of our clean sample are very similar to those applied by Loble *et al.* for the calculation of the XAS signal of Ce(III) in $CeCl_6^{3-}$ [36].

The good agreement between experimental and simulated spectra suggests that the ionic state for Ce ions in $CePdIn_2$ is predominantly 3+, which corresponds to a $4f$ level occupation number $n_f \simeq 1$, and it solidly points to local-moment character of the $4f$ electrons in this compound. This is supported by the quantitative results of the fitting of the Ce 3d PES core level spectrum presented later in this section. It is also worth mentioning that the fact that the XAS line shape resembles the calculation for Ce in its ionic form serves to confirm the nearly localised character/nature of the Ce $4f$ wave function in $CePdIn_2$.

However, at this stage the presence of a certain percentage of Ce atoms in the $4f^0$ (4+) ionic state in the bulk of the sample cannot be completely discarded, as it is known that XAS measurements in TEY have a certain contribution from the surface of the sample, for which the $4f^0$ spectral weight tends to be suppressed due to a reduced hybridization of the Ce $4f$ states with valence electrons at the surface [37]. Nevertheless, the Ce $M_{5,4}$ XAS spectrum constitutes a very good qualitative indication of the Ce valence.

The XAS spectrum for a contaminated $CePdIn_2$ sample is shown in Fig. 3(c) for reference purposes. The additional features (indicated by black arrows) visible in this spectrum are characteristic of the $4f^0$ initial state - corresponding to a 4+ ionic state for Ce [33] - and are a result of the surface contamination of the sample from the atmosphere. This is consistent with the fact that these features disappear in spectrum (a) for the scraped sample and appear again once the sample has aged in UHV, as shown in spectrum (d) in this figure. The appearance of similar features in the Ce $M_{5,4}$ XAS spectra due to surface contamination has also been reported, for example, for high-temperature superconductors $CeFeAsO_{1-x}F_x$ [38].

The Ce 3d core level spectrum for $CePdIn_2$ is shown in Fig. 4. The line shape of the core level is constituted by two sets of peaks corresponding to $3d_{5/2}$ and $3d_{3/2}$ spin-orbit states, whose centroids are located at binding energies of $\approx$ 884 eV and $\approx$ 902.5 eV respectively, separated by a spin-orbit splitting of 18.6 eV. The composition of the Ce 3d core level in Ce-based compounds derives from the fact that the initial ground state wave function ψ_0 of the $4f$ electrons can be written as a linear combination of three quantum mechanical states corresponding to the $4f^0$, $4f^1$ and $4f^2$ valence states of Ce, according to the

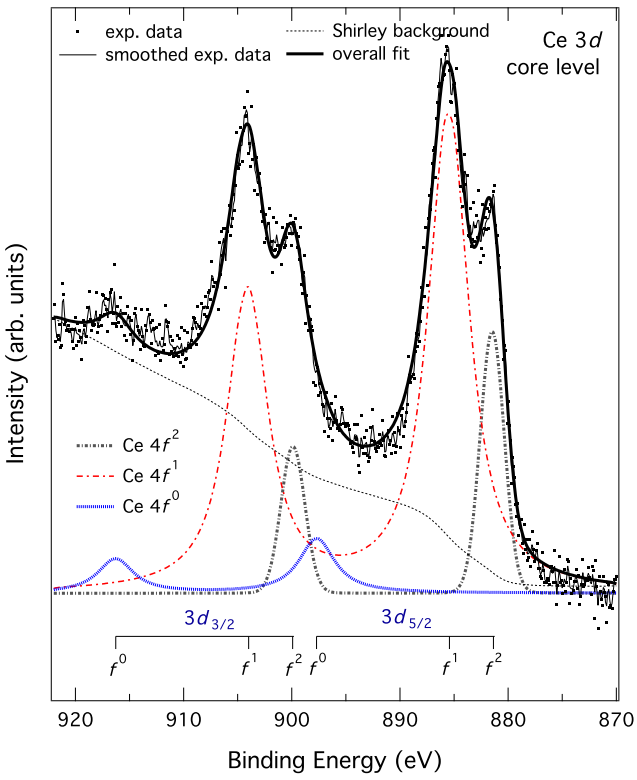

FIG. 4: (Color online) Ce 3d PES spectrum for $CePdIn_2$ measured with an incident photon energy of 1060 eV. The overall fit (thick black line) is constituted by the sum of the $4f^0$, $4f^1$ and $4f^2$ doublets together with a Shirley-type background, and it shows an overall good agreement with the experimental data points (black dots).

following relation: $\psi_0 = c_0\,|4f_0> + c_1\,|4f_1> + c_2\,|4f_2>$, where $|c_0|^2$, $|c_1|^2$ and $|c_2|^2$ can be related to the weight of the corresponding peaks in the core level spectrum. This has been extensively studied since the beginning of the 1980s [39, 40], and consequently it is very well understood. Therefore the Ce 3d line shape results from the superposition of three spin-orbit doublets ascribed to - from higher to lower binding energy - the $4f^0$, $4f^1$ and $4f^2$ valence states of Ce as mentioned above. These subcomponents are known to arise from the two different mechanisms with which the screening of the 3d core hole (resulting from the photoemission process) can occur for either the Ce $4f^0$ or the $4f^1$ states [41]. The so-called "poorly screened" channel is the one whereby the $4f$ orbital is screened by other electrons within the Ce atom itself; here the Ce atom is either in the $4f^0$ or in the $4f^1$ configuration. The "well-screened" channel is the one whereby the screening is performed by an electron that has been transferred to the Ce $4f$ orbital by the ligand/conduction band states; in this case the Ce atom is either in the $4f^1L^{-1}$ or in the $4f^2L^{-1}$ configuration, where L^{-1} is to remind us of the hole in the ligand/conduction band states [41]. The

latter mechanism is obviously favoured by a larger Ce $4f$ hybridization strength. It is important to underline at this point that the valence of Ce is determined by a linear combination of $4f^0$ and $4f^1$ states, i.e. it can range from 4+ to 3+. So the existence of an f^2 state is not to be attributed to a putative "2+" valence for Ce, but it is a signature of hybridization of the Ce $4f$ states with the conduction electrons [41], and the more intense the f^2 peak, the stronger the hybridization, i.e. the more effective is the mechanism of charge transfer described above.

Consistent with this model, the $3d$ core level PES spectrum has been fitted considering a Shirley-type background and three spin-orbit doublets representing $4f^2$, $4f^1$ and $4f^0$ states of Ce. The spin-orbit splitting has been kept fixed at 18.6 eV for all three subcomponents, and the branching ratio $I(3d_{5/2})/I(3d_{3/2})$ (expected to be 1.5 for a $3d$ core level) that best fitted the data was determined to be 1.56 for all 3 subcomponents. Such a deviation from the expected value for the branching ratio can be explained by the fact that this parameter can have some degree of anisotropy that may depend on the photon energy and the crystal structure [42]. The subcomponents as well as the overall fit are plotted in Fig. 4, showing a good agreement with the experimental data.

According to the model developed by Fuggle *et al.* [39] and Gunnarson and Schönhammer [40] (hereafter GS model), two very useful parameters can be extracted from the fitting of the Ce $3d$ core level: the hybridization energy Δ_{fs} between Ce $4f$ and conduction electrons, and the $4f$ level occupation n_f. In particular, Δ_{fs} can be estimated from the ratio:

$$r = \frac{I(f^2)}{I(f^1) + I(f^2)}, \tag{1}$$

and

$$n_f \simeq 1 - \frac{I(f^0)}{I(f^0) + I(f^1) + I(f^2)}, \tag{2}$$

where $I(f^0)$, $I(f^1)$ and $I(f^2)$ are the spectral intensities of the f^0, f^1 and f^2 components, respectively. The sign "$\simeq$" in Eq. 2 is used to remind us that this relationship is valid under the assumption that the mixing of the final-state configurations can be neglected for the f^0 state at least, and so the spectral weight of the f^0 component is a good representation of the value of $|c_0|^2$ described above [39]. This is acceptable if the relative spectral weight of the f^0 component constitutes less than 10% of the overall spectral weight of the Ce $3d$ core level photoemission spectrum, as is the case here.

Considering the intensities of the two relevant components, we obtain a value of $r \simeq 0.35$. Making use of the relationship between r and Δ_{fs} elucidated in Ref. [39], we obtain a value for $\Delta_{fs} = 180 \pm 5$ meV for $CePdIn_2$. The Ce $4f$ occupation number is found to be $n_f = 0.92 \pm 0.01$.

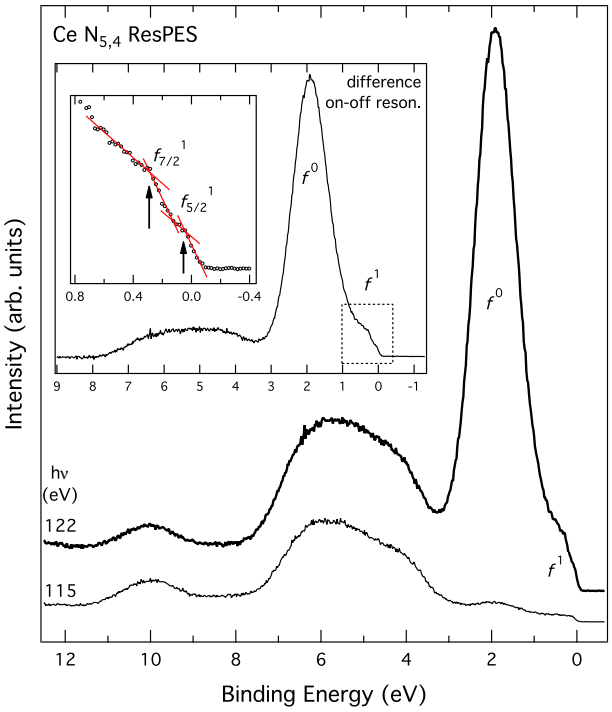

FIG. 5: (Color online) Valence band spectra acquired at hν = 115 eV (thin line) and at hν = 122 eV (thick line), corresponding to just before and to the maximum of the Ce $N_{5,4}$ resonance, respectively. The spectra have been normalized to the photon flux and offset for better clarity. The inset shows the difference between the on- and off- resonance valence bands, as well as the enlargement of the dashed region of difference spectrum in the proximity of E_F, where the $4f^1_{7/2}$ and $4f^1_{5/2}$ features are visible as the crossing points of the (red) lines fitting the various slopes of the spectrum.

An occupation number of 0.92 correlates well with an effective moment of 2.20 μ_B per Ce atom, as calculated from bulk magnetic measurements; this is discussed in Appendix 1 and the inverse magnetic susceptibility is shown in Fig. 8. n_f can be converted into an average valence of Ce ions $v_{Ce} = 3.08 \pm 0.01$.

Large values of Δ_{fs} in the presence of Pd are not unusual and have been documented before [43]. This can be ascribed to the large spatial delocalisation of the Pd $4d$ orbitals that would favour the overlap with the $4f$ states. The large value of Δ_{fs} for $CePdIn_2$ is however amongst the largest compared to other Ce intermetallic compounds with $4d$ elements as ligand atoms [39], and hints to the important role played by it in the description of the ground state properties of this system.

It is important at this point to comment on the possible surface contribution to the line shape of the Ce $3d$ core level spectrum. The kinetic energy of the photoelectrons in the Ce $3d$ core level spectrum displayed in Fig. 4 ranges from roughly 135 eV to 185 eV. This energy range is very

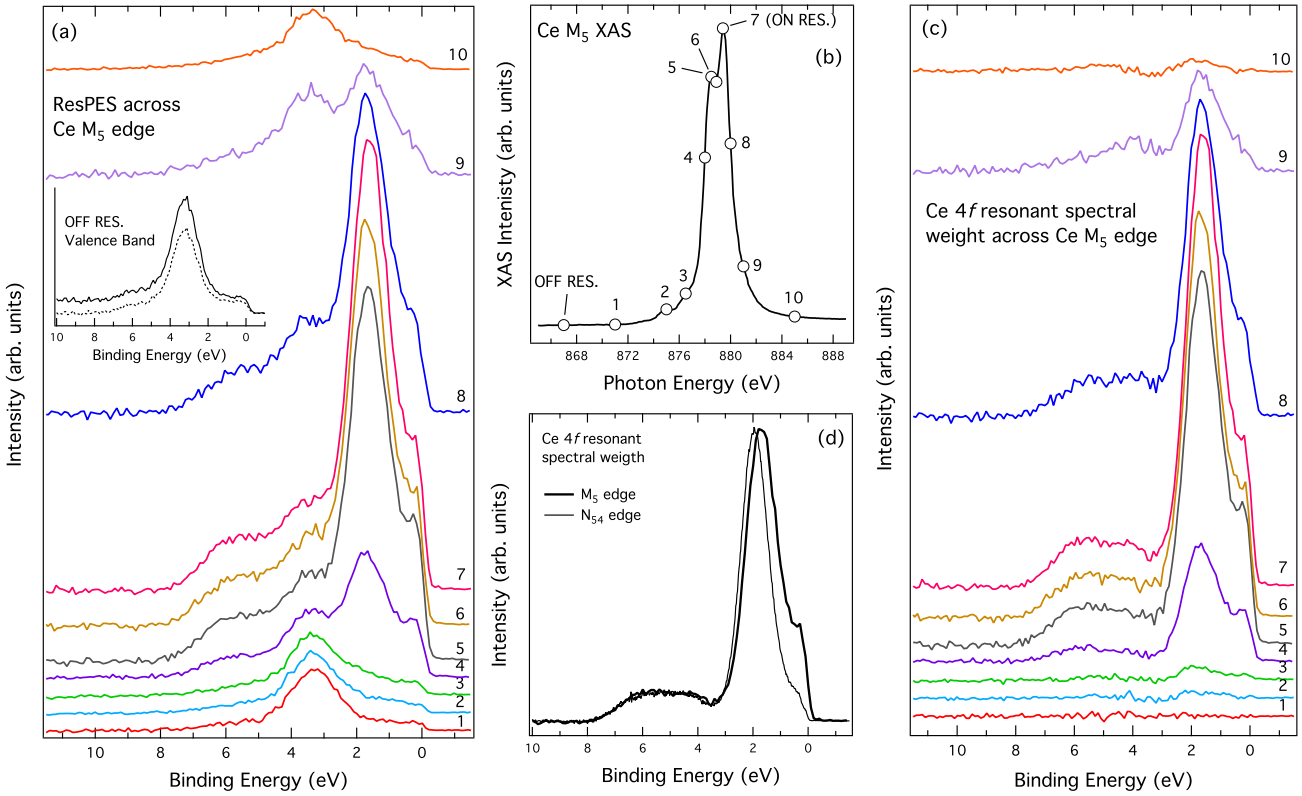

FIG. 6: (Color online) (a) Ce $3d_{5/2} - 4f$ ResPES series acquired with incident photon energies marked as circles on the corresponding XAS spectrum shown in (b) and labelled from 1 to 10. All spectra have been normalized to the incident flux and a Shirley background has been subtracted from each of them. The inset shows the valence band spectrum measured at h$\nu = 867$ eV (hereafter referred to as the 'off-resonance' valence band) before (solid lone) and after (dashed line) subtraction of a Shirley background. The on-resonance spectrum corresponds to photon energy 7 in (b). (c) Resonant valence band spectral weight obtained by subtracting the background-subtracted off-resonance spectrum (dashed line in the inset of panel (a)) from each valence band spectrum in (a). (d) Comparison between the Ce $4f$ resonant spectral weight obtained as the difference between on- and off-resonance spectra for the ResPES at both Ce M_5 and $N_{5,4}$ edges.

close to the minimum of the inelastic mean free path for photoelectrons reported in Refs. [44, 45]. Higher bulk sensitivity in photoemission spectra can be achieved by increasing the incident photon energy to several keV. A higher bulk sensitivity is usually reflected in the Ce $3d$ core level photoemission spectrum as a relative increase in the spectral weight of the $4f^0$ and $4f^2$ components with respect to the $4f^1$ component [46, 47]. $CePdIn_2$ can reasonably be expected to follow the same trend. Taking into account Eqns. 1 and 2, this will result in a slight increase of the value of Δ_{fs}, corresponding to a slight decrease of the value of n_f. We can therefore conclude that, because of the enhanced surface sensitivity of our measurements, our results provide an upper limit for n_f and a lower limit for the hybridization strength Δ_{fs}.

In order to investigate the contribution of the Ce $4f$ states to the valence band, we have performed ResPES measurements at both the $N_{5,4}$ and M_5 edges of Ce. This is done in order to take advantage of the enhancement of the cross section of the Ce $4f$ valence band states, and it allows to identify them amongst the other valence band states. Despite being both based upon the same resonance principle, the ResPES across the two edges are qualitatively different: the one across the $N_{5,4}$ edges is more surface sensitive (given the photon energies involved) but it allows for the acquisition of spectra with very good energy resolution in less amount of time, while the ResPES across the M_5 edge is more bulk sensitive [48] but it requires to compromise on the energy resolution of the spectra to allow for data acquisition in a reasonable amount of time. Despite these side effects, the information gathered from both techniques can be harmoniously combined in order to obtain a more general picture.

Let us then analyse the $N_{5,4}$ ResPES data first. Fig. 5 shows the on- and off-resonance valence band spectra acquired at photon energies of 122 eV and 115 eV, respectively. The off-resonance spectrum shows a broad peak centred at a binding energy of ~ 10 eV, followed by a

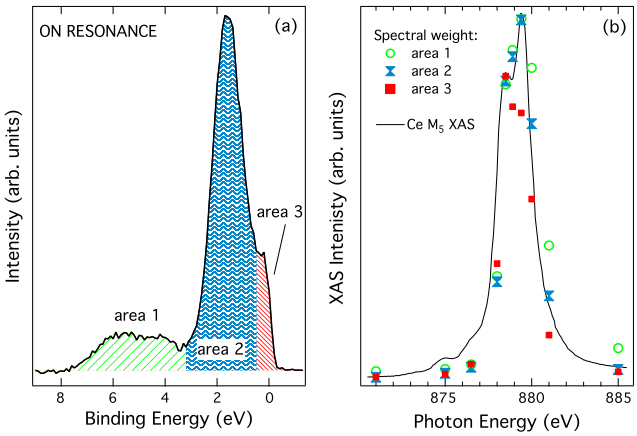

FIG. 7: (Color online) (a) Subdivision of the Ce $4f$ resonant spectral weight (measured with photon energy marked as 7 in figure 6(b)) in area 1, area 2 and area 3. Refer to the main text for further explanation. (b) Integrated intensity over areas 1, 2 and 3 plotted on top of the Ce M_5 XAS for direct comparison. All three integrated intensities have been normalized to better compare to the XAS spectrum.

broad feature ranging from 7.5 to 3 eV (with maxima at 6 and 4 eV), another feature at ~ 1.9 eV and a broad structure located just before the Fermi energy cut off. The line shape of the on-resonance spectrum resembles fairly well the off-resonance one, except for the very intense resonance in the spectral region within 3 eV from E_F. This is clearly visible in the inset of Fig. 5, which represents the $4f$ resonance spectral weight (RSW), i.e. the on-off resonance difference spectrum. Here we can see that the major part of the Ce $4f$ RSW extends over a wide region that goes from E_F down to about 3 eV binding energy. In particular, the RSW shows an intense feature centred at 1.92 eV, which can be attributed to the $4f^0$ states, while the spectral weight closer to E_F is due to the $4f^1$ states, and specifically to the $4f^1_{5/2}$ peak (also referred to as the tail of the Kondo resonance peak) located just below E_F and its spin-orbit counterpart $4f^1_{7/2}$. These features, as predicted by the SIAM model [40] and shown in our results, are consistent with the ResPES studies on many other Ce-based compounds [28, 46, 48–53]. Their spin-orbit splitting $\Delta_{SO} \simeq 240$ meV is also qualitatively in good agreement with the values reported for other Ce-based compounds [48, 54–58].

A closer look to the inset of Fig. 5 reveals that the RSW is not limited to the region from 3 eV binding energy to E_F, but it extends up to 7.5 eV from E_F. We are going to resume this issue later and to discuss it together with the results from the M_5 ResPES series presented below.

ResPES across the M_5 edge was performed in order to increase the bulk sensitivity to the measurements. Fig. 6(a) shows valence band spectra (after subtraction of a Shirley background) acquired across the $3d_{5/2} - 4f$ (M_5) threshold. The photon energies used are labelled from 1 to 10 and are indicated as open circles in the XAS spectrum (b). All spectra have been normalized to the incident photon flux. The inset shows what will be referred to as the 'off-resonance' valence band spectrum measured at 867 eV. This spectrum shows a broad intense peak at ~ 3.3 eV binding energy with a lower-intensity shoulder centred at about 6 eV, and a constant density of states from ~ 1.4 eV to E_F. A qualitative comparison with the density of states calculations performed for other Ce compounds containing Pd (i.e. $CePd_2$ [37], $CePd_3$ [37, 43] and $CePd_2Si_2$ [59]) allows us to state that these states can be ascribed mostly to the Pd $4d$ bands, although the presence of In states cannot be ruled out as no electronic structure calculations for $CePdIn_2$ are available to date. More specifically, the calculations presented in the above-cited articles consistently locate the majority of the Pd $4d$ states in the binding energy region above 2 eV, which agrees well with the location of the broad and more intense feature seen in the off-resonance valence band presented in the inset.

As the photon energy is increased across the absorption edge, we see a systematic enhancement of the spectral intensity between E_F and ~ 3 eV binding energy, reflecting to the resonance of the Ce $4f$ states. The maximum of the resonance occurs at $h\nu = 879.4$ eV - labeled as 7 in (b) - which corresponds to the most intense peak in the XAS spectrum. In order to make the $4f$ contribution to the valence band more visible, the background subtracted 'off-resonance' valence band spectrum shown in the inset of panel (a) has been subtracted from all spectra shown in the main panel (a). The difference spectra are shown in Fig. 6(c) for the same photon energies 1-10, and represent the $4f$ RSW across this absorption edge. This series of spectra clearly shows 1) a strong resonance below 3 eV binding energy, characterized by two features at roughly 1.9 eV and in close proximity of E_F, consistent with the location of the $4f_1$ and $4f_0$ peaks observed in the more surface sensitive $N_{5,4}$ ResPES; and 2) a weak RSW appearing as a broad structure between roughly 3 eV and 7.5 eV, again consistent with what was observed in the $N_{5,4}$ ResPES.

Fig. 6(d) shows a comparison between the RSW at the $N_{5,4}$ and M_5 edges. The spectra have been normalized to the maximum of the photoemission intensity for better comparison. The comparison clearly shows that the $4f^1/4f^0$ intensity ratio is enhanced in the more bulk sensitive M_5 ResPES. As this ratio increases with the hybridization strength between Ce $4f$ and conduction states [56], this result is to be expected as the hybridization is larger in the bulk of the material with respect to the surface. This has been shown to occur in other Ce-based systems [51, 60, 61].

Another common feature of the M_5 and the $N_{5,4}$ ResPES is the fact that the intensity of the $4f^0$ component is much higher than the $4f^1$ (roughly twice as intense for the

M_5 resonance, and more for the $N_{5,4}$ one). This seems to be a consistent feature in the ResPES of Ce alloys containing Pd [55, 56, 62, 63]. In particular, the reader is invited to compare the Ce $4f$ RSW of CeNiSn versus CePdSn [56] and of $CePd_2Si_2$ versus $CeNi_2Si_2$ [62], where it is clearly visible how the $4f^1$ peak is suppressed in the presence of Pd. Moreover, the intensity of the Kondo resonance peak is expected to increase while decreasing the temperature [57, 64] and approaching the Kondo temperature of the system.

An interesting fact revealed by the RSW in Fig. 6(d) is that both ResPES series show a resonant enhancement in the binding energy region from 3 to 7.5 eV. A similar observation has been reported in $CeAg_2Ge_2$ [65], even though the authors of this paper claim that the spectral weight present in this region does not show any clear resonance behaviour, and it is therefore not included in their analysis.

As in most of the spectroscopic investigations of the electronic structure of Ce-based compounds the attention is generally focused on the binding energy region from E_F to 3 eV (where the majority of the Ce $4f$ spectral weight is expected to be located), it is interesting to explore the behaviour of the valence band states at higher binding energy across the Ce resonance. Before commenting further on this issue, we would like to provide evidence that ours is a genuine result, and not an artefact due to the contamination of the surface. For this purpose, we invite the reader to consult the material published in the Supplementary Information, where it is clearly shown that the effect of the surface contamination on the photoemission intensity from the valence band at binding energies higher than 3 eV is to develop some additional spectral weight in an energy region limited to the [3.5 - 5] eV. This is certainly not enough to justify what is seen in our analysis.

Some clarification in this regard can be sought from the evaluation of the behaviour of the valence band states across the Ce M_5 resonance. We have therefore divided the RSW into three energy regions, as shown in Fig. 7(a), where area 1, area 2 and area 3 represent the energy regions from 3 to 7.5 eV, from 0.5 to 3 eV ($4f^0$ states) and from -0.5 to 0.5 eV ($4f^1$ states), respectively. For each of them we have calculated the integral of the spectral intensity across the M_5 edge and plotted them in Fig. 7(b) together with the Ce M_5 XAS. This direct comparison shows that all three areas resemble quite well the features of the XAS spectrum, the only major discrepancy being the integral for area 3 showing a dip at the photon energy corresponding to the maximum absorption intensity. In the absence of density of states calculations for this compound, we can speculate that the fact that the integrated intensity for area 1 shows a trend similar to the XAS spectrum is an indication of the presence of Ce $4f$ character in this energy region. The presence of $4f$ density of states at binding energies higher than 3-4 eV has been excluded by the electronic structure calculations performed on a number of Ce-based compounds (consider for example $Ce_2(Co/Rh)Si_3$ [64, 66], $Ce(Fe/Ru/Os)_2Al_{10}$ [27], $CeAg_2Ge_2$ [65], $CeFe_2$ [67], $CeFe_4P_{12}$ [46], $CeRhSb_{1-x}Sn_x$ [68], to cite a few). For the instances where it was predicted [37, 43, 69], it was consistently very marginal with respect to the near-E_F region, and could not justify for the RSW to correspond to almost 20% of the overall Ce $4f$ RSW, as is found here.

Our observation can therefore be justified as an effect occurring through the strong hybridization of the $4f$ states with the ligand states, that are mostly located in this higher binding energy region, as discussed earlier with regards to the inset in Fig. 6(a). These ligand states could either be the $4d$ electrons of Pd or the $5p$ electrons of In. Pd valence electrons can be reasonably expected to have a larger hybridization with the $4f$ states than In, as according to Ijiri *et al.* [7] Ce-Pd bond lengths are at least $\sim 10\%$ shorter than the Ce-In ones.

We can qualitatively justify our claim by looking at the results for the detailed electronic structure calculations for $CePd_3$ in Ref. [43]. Figure 3 of this article shows that the energy region occupied by Pd $4d$ states extends down to about 7 eV from E_F, and the majority is located above 1.5 eV, while the majority of the Ce $4f$ states is located from 1.5 eV to E_F. Interestingly for us, the calculation of the f-d hybridization strength for this compound shown in Figure 2 of the same article reveals that the hybridization strength is weak in the energy region above 1.5 eV to E_F, while it becomes very large in the energy region occupied by the $4d$ states of Pd, to the point of showing two peaks corresponding to the maxima of the Pd $4d$ bands. In a similar study performed for $CeIn_3$ [70], the same author shows that the hybridization strength between $4f$ electrons and In valence states is at least five times smaller than in the case of Pd. This might be the case for $CePdIn_2$, even though we can not definitively claim so based on the available information. It should however be noted that the shape of the off-resonance valence band shown in the inset of Fig. 6(a) is different from the shape of the resonant spectral weight shown in Fig. 6(d), even though the extension to binding energy of roughly 7.5 eV is consistent between them. The reason for the different behavior of the Pd $4d$ states across the Ce resonance can be only speculated about at this stage. One reason for this could be the binding energy dependence of the hybridization strength between Pd $4d$ and Ce $4f$ states, even though this should be confirmed by electronic structure calculations.

Based on the discussion above and on the large value of the hybridization strength found from the fit of the Ce $3d$ core level, we feel justified to attribute the $4f$ RSW in the binding energy region between 3 eV and 7.5 eV to the f-d strongly hybridized states. This suggests the fundamental role played by the indirect exchange between localized $4f$ states mediated by d electrons, which could possibly

favour long range ferromagnetism at lower temperatures as well as the deviation from trivalency, consistently with the specific heat results reported later in the Appendix. Our results are consistent with the work by Batista et. al. [71, 72], where it is shown that in the strong coupling limit the hybridization between f- and d-electron bands leads to a ferromagnetic ground state possibly of itinerant nature.

CONCLUSIONS

In summary, we have investigated the Ce $4f$ contribution to the electronic structure of $CePdIn_2$ by means of XAS at the Ce $M_{5,4}$ edges, PES from Ce $3d$ core level and ResPES at the Ce $N_{5,4}$ and $M_{5,4}$ edges, performed on polycrystalline samples at room temperature. The Ce $4f$ occupation number is found to be 0.92, indicating that the vast majority (more than 90%) of the Ce ions have a 3+ charge state. This is also consistent with an effective magnetic moment of 2.20 μ_B per Ce ion as found from the inverse magnetic susceptibility, that corresponds to $\sim 87\%$ of that for a free-ion, as well as with the line shape of the Ce $3d$ - $4f$ XAS that shows very good agreement with that for atomic Ce^{3+} valence state. The analysis of the two ResPES series shows in a consistent manner that the Ce $4f$ states are composed of the features predicted by the single impurity Anderson model, i.e. a broad $4f^0$ peak centred at a binding energy of 1.9 eV and two $4f^1$ spin-orbit states much closer to the Fermi level separated by a spin orbit coupling of roughly 240 meV. The $4f^1/4f^0$ intensity ratio is enhanced in the more bulk sensitive M_5 ResPES, as a result of the fact that the hybridization is larger in the bulk of the material with respect to the surface. Furthermore, the ResPES at both edges reveal that the $4f$ resonant spectral weight extends to the deeper regions of the valence band, i.e. at binding energies larger than 3 eV, that is presumably occupied by the Pd $4d$ ligand states. We interpret this as a signature for the strong f-d hybridization present in the system, consistent with the large value of ~ 180 meV found from the analysis of the Ce $3d$ core level. This could possibly favour the emergence of long range ferromagnetism through the indirect exchange between localized $4f$ states mediated by highly dispersive d electrons.

Acknowledgements

This work is based on the research supported in part by the South African National Research Foundation (SA-NRF) through Grant No 90698, and in part by the SISTER-MAE programme. AMS thanks the SA-NRF (Grant No 93549), and the URC and FRC of the University of Johannesburg for financial support. XRD and SEM measurements were performed with the instrumentation available at the Spectrum Analysis Facility of the University of Johannesburg, whose staff is hereby acknowledged for technical support. Finally, the authors would also like to thank Elettra for the provision of the beamtime as user proposal no. 20140044.

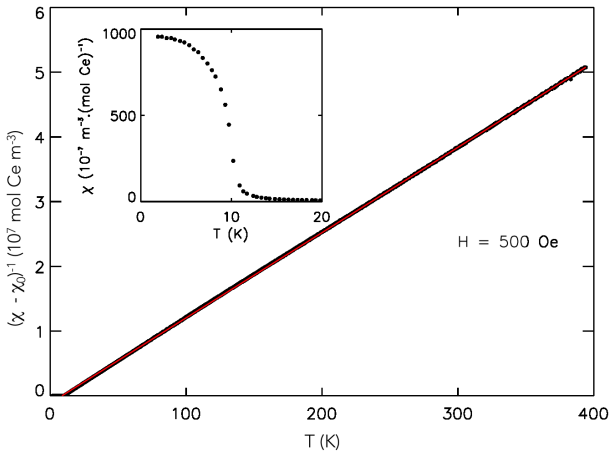

FIG. 8: (Color online) Inverse magnetic susceptibility of $CePdIn_2$ (black circles) after the subtraction of a small temperature independent contribution. Curie-Weiss behaviour above 10 K is evidenced by the good agreement of the data with the fitted red solid line. Inset: Magnetic susceptibility in the vicinity of $T_C = 10$ K.

Appendix 1: Inverse magnetic susceptibility of $CePdIn_2$

The inverse magnetic susceptibility $\chi^{-1}(T)$ of $CePdIn_2$ is shown in Fig. 8, together with the magnetic susceptibility in the vicinity of T_C. The magnetic susceptibility is calculated from a field-cooled magnetisation measurement using a background magnetic field of 500 Oe. Above the magnetic transition temperature the inverse magnetic susceptibility can be fitted to the modified Curie-Weiss law

$$\chi(T) = \frac{N_A}{3k}\frac{\mu_{eff}^2}{T-\Theta_p} + \chi_0\,, \qquad (3)$$

where μ_{eff} is the effective magnetic moment, Θ_p is the paramagnetic Weiss temperature and χ_0 accounts for possible temperature independent contributions to the magnetic susceptibility. The solid line in Fig. 8 shows the best fit of equation 3 to the experimental data above 200 K. The following values were extracted from the fit: $\Theta_p = 8.6$ K (very close to the observed value of T_C), $\chi_0 = -1.08\times10^{-9}$m^3.mol Ce^{-1} and $\mu_{eff} = 2.20\,\mu_B$ per Ce ion. Above 200 K the average deviation between the fitted and experimental curves is $\langle\delta_\chi\rangle = 7.30\times10^{-11}$m^3.mol Ce^{-1}. Below 200 K a slight deviation from Curie-Weiss behaviour is found, possibly due to CEF effects.

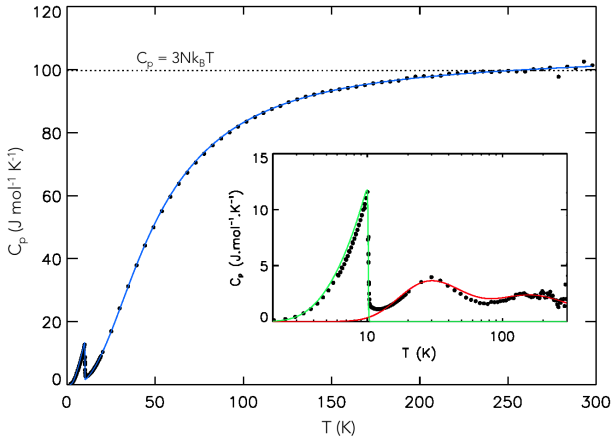

FIG. 9: (Color online) The specific heat of $CePdIn_2$ (filled circles) together with a numerical fit (solid blue line) as described in the text. Inset: $4f$ electron contribution to the specific heat (filled circles). The solid lines show the magnetic configurational specific heat of a model mean field spin-1/2 ferromagnet as well as the calculated Schottky contribution arising from the thermal population of CEF split levels as reported in the text.

A value of $2.20\,\mu_B$ for the effective moment is $\sim 87\%$ of the expected free-ion value, which is in very good agreement with the value of 0.92 calculated for the $3d$ core level above. For Ce-based compounds an effective paramagnetic moment smaller than the free-ion value at high temperatures is often an indication of a departure from tri-valency due to hybridization effects between the $4f$ and conduction electron states. This departure is accompanied by a loss of the 'local moment' character of the $4f$ electrons.

Appendix 2: Specific heat of $CePdIn_2$

The specific heat $C_P(T)$ of $CePdIn_2$ is shown in Fig. 9. With increasing temperature towards 300 K, $C_P(T)$ approaches the classic Dulong-Petit limit (dashed line in Fig. 9) in the case of four atoms per formula unit. Below 300 K $C_P(T)$ shows a typically phonon dominated shape, while a sharply defined anomaly emerges at $T_C = 10\,\mathrm{K}$, consistent with magnetic ordering as reported in earlier studies [7, 8]. A good fit to the data in Fig. 9 is found by considering phononic, electronic, CEF and magnetic configurational contributions to $C_P(T)$. The fit depends on the Debye temperature Θ_D, Sommerfeld coefficient γ, CEF excitation energies Δ_1 and Δ_2 (assuming a six-fold free-ion ground state degeneracy, which can be uplifted into, at most, three doublets), as well as the ferromagnetic transition temperature T_C. The Sommerfeld coefficient represents the free electron weight at the Fermi level, and it parameterises this contribution to the specific heat through $C_{el} = \gamma T$. The CEF excitation energies describe the relative position of two excited doublets above an assumed doublet $4f$ electron ground state. The thermal population of the CEF split energy levels produces the characteristic Schottky-type features in the specific heat (clearly shown in the inset of Fig. 9). It is important to note that in our fit Δ_1 and Δ_2 were allowed to vary between 0 K and 500 K. Lastly, T_C parameterises the purely magnetic configurational specific heat of a mean field ferromagnet (with two assumed moment orientations). The fit was performed by means of a stochastic algorithm designed to generate random instances of the parameters described above. For every 200000 instances the parameter set that gave the best fit to the experimental data was binned. The whole procedure was repeated 30 times, yielding the 30 best parameter sets, for which the average value was taken.

Our parametrisation revealed a small electronic contribution above T_C, characterized by a Sommerfeld coefficient $\gamma = 16\,\mathrm{J.mol^{-1}.K^{-2}}$. This value is typically metallic and of the same order of magnitude as that reported in Ref. [8]. Furthermore, the above-mentioned procedure yields $\Theta_D = 205 \pm 2\,\mathrm{K}$ and $\Delta_1/k_B = 72 \pm 10\,\mathrm{K}$, similar to the values reported in an earlier independent study [8]. We find that the second CEF excitation Δ_2 lies $438 \pm 30\,\mathrm{K}$ above the ground state. This is at odds with the value of 110 K reported in Ref. [8], where $C_P(T)$ is only reported up to 100 K. Subtraction of the phononic and Sommerfeld contributions to the specific heat yields the data shown in the inset of Fig. 9, which we use as an estimate of the $4f$ electron contribution to the specific heat, i.e. C_{4f}. As shown, the two broad maxima towards higher temperatures are well described by the CEF level dispensation proposed here. Also shown in the inset is the magnetic configurational specific heat of a mean field ferromagnet (with two allowed moment orientations per site). At 10 K and below, the mean field model calculation mirrors the experimental C_{4f} data extremely well, leading us to conclude that $CePdIn_2$ is a mean field ferromagnet.

* Electronic address: ecarleschi@uj.ac.za

[1] Q. Si and F. Steglich, Science **329**, 1161 (2010), URL http://www.sciencemag.org/content/329/5996/1161.abstract.

[2] T. Park, F. Ronning, H. Q. Yuan, M. B. Salamon, R. Movshovich, J. L. Sarrao, and J. D. Thompson, Nature **440**, 65 (2006), URL http://dx.doi.org/10.1038/nature04571.

[3] S. Doniach, Physica B+C **91**, 231 (1977), URL http://www.sciencedirect.com/science/article/pii/0378436377901905.

[4] D. Shtepa, S. Nesterenko, A. Tursina, E. Murashova, and Y. Seropegin, Moscow University Chemistry Bulletin **63**, 162 (2008), URL http://dx.doi.org/10.3103/S0027131408030048.

[5] E. Brück, M. van Sprang, J. C. P. Klaasse, and F. R. de Boer, Journal of Applied Physics **63**, 3417 (1988), URL http://scitation.aip.org/content/aip/journal/jap/63/8/10.1063/1.340751.

[6] K. Satoh, T. Fujita, Y. Maeno, Y. Uwatoko, and H. Fujii, Journal of the Physical Society of Japan **59**, 692 (1990), URL http://jpsj.ipap.jp/link?JPSJ/59/692/.

[7] Y. Ijiri, F. DiSalvo, and H. Yamane, Journal of Solid State Chemistry **122**, 143 (1996), URL http://www.sciencedirect.com/science/article/pii/S0022459696900948.

[8] L. da Silva, A. dos Santos, M. de Melo, L. Cardoso, A. Medina, and F. Gandra, Physica B: Condensed Matter **404**, 3018 (2009), URL http://www.sciencedirect.com/science/article/pii/S0921452609005328.

[9] A. Bianchi, E. Felder, A. Schilling, M. Chernikov, F. Hulliger, and H. Ott, Zeitschrift für Physik B Condensed Matter **99**, 69 (1995), URL http://dx.doi.org/10.1007/s002570050012.

[10] S. Mock, T. Pietrus, A. Sidorenko, R. Vollmer, and H. Löhneysen, Journal of Low Temperature Physics **104**, 95 (1996), URL http://dx.doi.org/10.1007/BF00754091.

[11] B. K. Cho, R. A. Gordon, C. D. W. Jones, F. J. DiSalvo, J. S. Kim, and G. R. Stewart, Physical Review B **57**, 15191 (1998), URL http://link.aps.org/doi/10.1103/PhysRevB.57.15191.

[12] V. I. Zaremba, U. C. Rodewald, Y. M. Kalychak, Y. V. Galadzhun, D. Kaczorowski, R.-D. Hoffmann, and R. Pöttgen, Zeitschrift für Anorganische und Allgemeine Chemie **629**, 434 (2003), URL http://dx.doi.org/10.1002/zaac.200390072.

[13] A. Tursina, S. Nesterenko, E. Murashova, Z. Kurenbaeva, Y. Seropegin, H. Noël, T. Roisnel, and D. Kaczorowski, Intermetallics **19**, 1864 (2011), URL http://www.sciencedirect.com/science/article/pii/S0966979511002524.

[14] H. Kaldarar, E. Royanian, H. Michor, G. Hilscher, E. Bauer, A. Gribanov, D. Shtepa, P. Rogl, A. Grytsiv, Y. Seropegin, et al., Physical Review B **79**, 205104 (2009), URL http://link.aps.org/doi/10.1103/PhysRevB.79.205104.

[15] D. Kaczorowski, A. P. Pikul, D. Gnida, and V. H. Tran, Physical Review Letters **103**, 027003 (2009), URL http://link.aps.org/doi/10.1103/PhysRevLett.103.027003.

[16] J. K. Dong, H. Zhang, X. Qiu, B. Y. Pan, Y. F. Dai, T. Y. Guan, S. Y. Zhou, D. Gnida, D. Kaczorowski, and S. Y. Li, Phys. Rev. X **1**, 011010 (2011), URL http://link.aps.org/doi/10.1103/PhysRevX.1.011010.

[17] M. Matusiak, D. Gnida, and D. Kaczorowski, Physical Review B **84**, 115110 (2011), URL http://link.aps.org/doi/10.1103/PhysRevB.84.115110.

[18] M. Falkowski and A. M. Strydom, Journal of Alloys and Compounds **613**, 204 (2014), ISSN 0925-8388, URL http://www.sciencedirect.com/science/article/pii/S0925838814011529.

[19] K. Uhlířová, J. Prokleška, and V. Sechovský, Phys. Rev. Lett. **104**, 059701 (2010), URL http://link.aps.org/doi/10.1103/PhysRevLett.104.059701.

[20] D. Kaczorowski, A. P. Pikul, D. Gnida, and V. H. Tran, Phys. Rev. Lett. **104**, 059702 (2010), URL http://link.aps.org/doi/10.1103/PhysRevLett.104.059702.

[21] T. Mito, S. Kawasaki, Y. Kawasaki, G. q. Zheng, Y. Kitaoka, D. Aoki, Y. . Haga, and Y. Ōnuki, Phys. Rev. Lett. **90**, 077004 (2003), URL http://link.aps.org/doi/10.1103/PhysRevLett.90.077004.

[22] S.-i. Fujimori, A. Fujimori, K. Shimada, T. Narimura, K. Kobayashi, H. Namatame, M. Taniguchi, H. Harima, H. Shishido, S. Ikeda, et al., Phys. Rev. B **73**, 224517 (2006), URL http://link.aps.org/doi/10.1103/PhysRevB.73.224517.

[23] T. Takahashi, N. Sato, T. Yokoya, A. Chainani, T. Morimoto, and T. Komatsubara, Journal of the Physical Society of Japan **65**, 156 (1996), URL http://dx.doi.org/10.1143/JPSJ.65.156.

[24] N. K. Sato, N. Aso, K. Miyake, R. Shiina, P. Thalmeier, G. Varelogiannis, C. Geibel, F. Steglich, P. Fulde, and T. Komatsubara, Nature **410**, 340 (2001), URL http://www.nature.com/nature/journal/v410/n6826/abs/410340a0.html.

[25] S.-I. Fujimori, Y. Saitoh, T. Okane, A. Fujimori, H. Yamagami, Y. Haga, E. amamoto, and Y. Onuki, Nature Physics **3**, 618 (2007), URL http://www.nature.com/nphys/journal/v3/n9/full/nphys651.html.

[26] J. Goraus and A. Ślebarski, Journal of Physics: Condensed Matter **24**, 095503 (2012), URL http://stacks.iop.org/0953-8984/24/i=9/a=095503.

[27] S.-i. Kimura, T. Iizuka, H. Miyazaki, T. Hajiri, M. Matsunami, T. Mori, A. Irizawa, Y. Muro, J. Kajino, and T. Takabatake, Phys. Rev. B **84**, 165125 (2011), URL http://link.aps.org/doi/10.1103/PhysRevB.84.165125.

[28] A. Chainani, M. Matsunami, M. Taguchi, R. Eguchi, Y. Takata, M. Oura, S. Shin, K. Sengupta, E. V. Sampathkumaran, T. Doert, et al., Physical Review B **89**, 235117 (2014), URL http://link.aps.org/doi/10.1103/PhysRevB.89.235117.

[29] D. Kaczorowski and A. Ślebarski, Physical Review B **81**, 214411 (2010), URL http://link.aps.org/doi/10.1103/PhysRevB.81.214411.

[30] A. C. Larson and R. B. Von Dreele, Los Alamos National Laboratory Report LAUR pp. 86–748 (1994).

[31] B. H. Toby, Journal of Applied Crystallography **34**, 210 (2001), URL http://dx.doi.org/10.1107/S0021889801002242.

[32] M. Zangrando, M. Zacchigna, M. Finazzi, D. Cocco, R. Rochow, and F. Parmigiani, Review of Scientific Instruments **75**, 31 (2004), URL http://scitation.aip.org/content/aip/journal/rsi/75/1/10.1063/1.1634355.

[33] B. T. Thole, G. van der Laan, J. C. Fuggle, G. A. Sawatzky, R. C. Karnatak, and J.-M. Esteva, Physical Review B **32**, 5107 (1985), URL http://link.aps.org/doi/10.1103/PhysRevB.32.5107.

[34] R. D. Cowan, *The Theory of Atomic Structure and Spectra;* (University of California Press, 1981).

[35] E. Stavitski and F. M. de Groot, Micron **41**, 687 (2010), URL http://www.sciencedirect.com/science/article/pii/S0968432810001423.

[36] M. W. Löble, J. M. Keith, A. B. Altman, S. C. E. Stieber, E. R. Batista, K. S. Boland, S. D. Conradson, D. L. Clark, J. Lezama Pacheco, S. A. Kozimor, et al., Journal of the American Chemical Society **137**, 2506 (2015), URL http://dx.doi.org/10.1021/ja510067v.

[37] L. Severin and B. Johansson, Physical Review B **50**, 17886 (1994), URL http://link.aps.org/doi/10.1103/PhysRevB.50.17886.

[38] F. Bondino, E. Magnano, C. H. Booth, F. Offi, G. Panac-

cione, M. Malvestuto, G. Paolicelli, L. Simonelli, F. Parmigiani, M. A. McGuire, et al., Physical Review B **82**, 014529 (2010), URL http://link.aps.org/doi/10.1103/PhysRevB.82.014529.

[39] J. C. Fuggle, F. U. Hillebrecht, Z. Zołnierek, R. Lässer, C. Freiburg, O. Gunnarsson, and K. Schönhammer, Physical Review B **27**, 7330 (1983), URL http://link.aps.org/doi/10.1103/PhysRevB.27.7330.

[40] O. Gunnarsson and K. Schönhammer, Physical Review B **28**, 4315 (1983), URL http://link.aps.org/doi/10.1103/PhysRevB.28.4315.

[41] F. de Groot and A. Kotani, in *Core level spectroscopy of solids* (CRC Press, 2008), Advances in Condensed Matter Science, URL http://www.crcpress.com/product/isbn/9780849390715.

[42] H. Yeom, T. Abukawa, Y. Takakuwa, S. Fujimori, T. Okane, Y. Ogura, T. Miura, S. Sato, A. Kakizaki, and S. Kono, Surface Science **395**, L236 (1998), URL http://www.sciencedirect.com/science/article/pii/S0039602897008327.

[43] O. Sakai, Journal of the Physical Society of Japan **79**, 114701 (2010), URL http://dx.doi.org/10.1143/JPSJ.79.114701.

[44] S. Tanuma, C. J. Powell, and D. R. Penn, Surface and Interface Analysis **25**, 25 (1997), ISSN 1096-9918, URL http://dx.doi.org/10.1002/(SICI)1096-9918(199701)25:1<25::AID-SIA207>3.0.CO;2-2.

[45] C. J. Powell and A. Jablonski, Surface and Interface Analysis **29**, 108 (2000), ISSN 1096-9918, URL http://dx.doi.org/10.1002/(SICI)1096-9918(200002)29:2<108::AID-SIA700>3.0.CO;2-4.

[46] M. Matsunami, K. Horiba, M. Taguchi, K. Yamamoto, A. Chainani, Y. Takata, Y. Senba, H. Ohashi, M. Yabashi, K. Tamasaku, et al., Physical Review B **77**, 165126 (2008), URL http://link.aps.org/doi/10.1103/PhysRevB.77.165126.

[47] L. Braicovich, N. B. Brookes, C. Dallera, M. Salvietti, and G. L. Olcese, Phys. Rev. B **56**, 15047 (1997), URL http://link.aps.org/doi/10.1103/PhysRevB.56.15047.

[48] A. Sekiyama, T. Iwasaki, K. Matsuda, Y. Saitoh, Y. Ônuki, and S. Suga, Nature **403**, 396 (2000), URL http://www.nature.com/nature/journal/v403/n6768/full/403396a0.html.

[49] T. Ishiga, T. Wakita, R. Yoshida, H. Okazaki, K. Tsubota, M. Sunagawa, K. Uenaka, K. Okada, H. Kumigashira, M. Oshima, et al., Journal of the Physical Society of Japan **83**, 094717 (2014), URL http://dx.doi.org/10.7566/JPSJ.83.094717.

[50] S. Banik, A. Arya, A. Bendounan, M. Maniraj, A. Thamizhavel, I. Vobornik, S. K. Dhar, and S. K. Deb, Journal of Physics: Condensed Matter **26**, 335502 (2014), URL http://stacks.iop.org/0953-8984/26/i=33/a=335502.

[51] H. J. Im, T. Ito, J. B. Hong, S.-i. Kimura, and Y. S. Kwon, Physical Review B **72**, 220405 (2005), URL http://link.aps.org/doi/10.1103/PhysRevB.72.220405.

[52] S. Raj, Y. Iida, S. Souma, T. Sato, T. Takahashi, H. Ding, S. Ohara, T. Hayakawa, G. F. Chen, I. Sakamoto, et al., Physical Review B **71**, 224516 (2005), URL http://link.aps.org/doi/10.1103/PhysRevB.71.224516.

[53] H. Ishii, T. Miyahara, Y. Takayama, H. Shiozawa, K. Obu, T. D. Matsuda, Y. Aoki, H. Sugawara, and H. Sato, Journal of Electron Spectroscopy and Related Phenomena **144-147**, 643 (2005), URL http://www.sciencedirect.com/science/article/pii/S036820480500109X.

[54] H.-D. Kim, O. Tjernberg, G. Chiaia, H. Kumigashira, T. Takahashi, L. Duò, O. Sakai, M. Kasaya, and I. Lindau, Physical Review B **56**, 1620 (1997), URL http://link.aps.org/doi/10.1103/PhysRevB.56.1620.

[55] T. Iwasaki, S. Suga, S. Imada, A. Sekiyama, T. Muro, S. Ueda, M. Saeki, H. Harada, T. Matsushita, H. Ishii, et al., Journal of the Physical Society of Japan **68**, 1716 (1999), URL http://dx.doi.org/10.1143/JPSJ.68.1716.

[56] A. Sekiyama, S. Suga, T. Iwasaki, S. Ueda, S. Imada, Y. Saitoh, T. Yoshino, D. Adroja, and T. Takabatake, Journal of Electron Spectroscopy and Related Phenomena **114-116**, 699 (2001), URL http://www.sciencedirect.com/science/article/pii/S0368204800003261.

[57] D. Ehm, S. Hüfner, F. Reinert, J. Kroha, P. Wölfle, O. Stockert, C. Geibel, and H. v. Löhneysen, Physical Review B **76**, 045117 (2007), URL http://link.aps.org/doi/10.1103/PhysRevB.76.045117.

[58] S. Patil, A. Generalov, and A. Omar, Journal of Physics: Condensed Matter **25**, 382205 (2013), URL http://stacks.iop.org/0953-8984/25/i=38/a=382205.

[59] M. Gomez Berisso, O. Trovarelli, P. Pedrazzini, G. Zwicknagl, C. Geibel, F. Steglich, and J. G. Sereni, Physical Review B **58**, 314 (1998), URL http://link.aps.org/doi/10.1103/PhysRevB.58.314.

[60] H.-D. Kim, H. Kumigashira, S.-H. Yang, T. Takahashi, H. Aoki, T. Suzuki, G. Chiaia, O. Tjernberg, H. Nylén, I. Lindau, et al., Physical Review B **59**, 12294 (1999), URL http://link.aps.org/doi/10.1103/PhysRevB.59.12294.

[61] A. Sekiyama, K. Kadono, K. Matsuda, T. Iwasaki, S. Ueda, S. Imada, S. Suga, R. Settai, H. Azuma, Y. Ōnuki, et al., Journal of the Physical Society of Japan **69**, 2771 (2000), URL http://dx.doi.org/10.1143/JPSJ.69.2771.

[62] K. Mimura, Y. Okabayashi, H. Mizohata, D. Sakiyama, O. Sakai, D. Huo, J. Sakurai, Y. Taguchi, K. Ichikawa, and O. Aita, Surface Review and Letters **9**, 1035 (2002), URL http://www.worldscientific.com/doi/abs/10.1142/S0218625X02003305.

[63] S. Kasai, S. Imada, A. Yamasaki, A. Sekiyama, F. Iga, M. Kasaya, and S. Suga, Journal of Electron Spectroscopy and Related Phenomena **156-158**, 441 (2007), URL http://www.sciencedirect.com/science/article/pii/S0368204807000138.

[64] S. Patil, V. R. R. Medicherla, R. S. Singh, E. V. Sampathkumaran, and K. Maiti, Europhysics Letters **97**, 17004 (2012), URL http://stacks.iop.org/0295-5075/97/i=1/a=17004.

[65] S. Banik, A. Chakrabarti, D. A. Joshi, A. Thamizhavel, D. M. Phase, S. K. Dhar, and S. K. Deb, Phys. Rev. B **82**, 113107 (2010), URL http://link.aps.org/doi/10.1103/PhysRevB.82.113107.

[66] S. Patil, V. R. R. Medicherla, R. S. Singh, S. K. Pandey, E. V. Sampathkumaran, and K. Maiti, Phys. Rev. B **82**, 104428 (2010), URL http://link.aps.org/doi/10.1103/PhysRevB.82.104428.

[67] T. Konishi, K. Morikawa, K. Kobayashi, T. Mizokawa, A. Fujimori, K. Mamiya, F. Iga, H. Kawanaka, Y. Nishihara, A. Delin, et al., Phys. Rev. B **62**, 14304 (2000), URL http://link.aps.org/doi/10.1103/PhysRevB.62.14304.

[68] A. Ślebarski, T. Zawada, J. Spałek, and A. Jezierski,

Physical Review B **70**, 235112 (2004), URL http://link.aps.org/doi/10.1103/PhysRevB.70.235112.

[69] N. C. Shekar, M. Rajagopalan, J. Meng, D. Polvani, and J. Badding, Journal of Alloys and Compounds **388**, 215 (2005), URL http://www.sciencedirect.com/science/article/pii/S092583880400965X.

[70] O. Sakai and H. Harima, Journal of the Physical Society of Japan **81**, 024717 (2012), URL http://dx.doi.org/10.1143/JPSJ.81.024717.

[71] C. D. Batista, J. Bonča, and J. E. Gubernatis, Physical Review Letters **88**, 187203 (2002), URL http://link.aps.org/doi/10.1103/PhysRevLett.88.187203.

[72] C. D. Batista, J. Bonča, and J. E. Gubernatis, Phys. Rev. B **68**, 214430 (2003), URL http://link.aps.org/doi/10.1103/PhysRevB.68.214430.